6726 *Chem. Mater.* **2010,** *22,* 6726–6735
DOI:10.1021/cm102724k

CHEMISTRY OF MATERIALS
Article

Fluorination of Iron Hexagonal Perovskites Promoting Low Temperature Oxygen Mobility

Mihai Sturza, Sylvie Daviero-Minaud, Houria Kabbour, Olivier Gardoll, and Olivier Mentré*

Université Lille Nord de France, Unité de Catalyse et de Chimie du Solide, CNRS UMR 8181, F-59652 Villeneuve d'Ascq cedex, France

Received September 21, 2010. Revised Manuscript Received November 5, 2010

New materials with original mechanisms driving low temperature oxygen mobility in solids are needed to reduce the operating temperature of solid-oxide fuel cells. Instead of the standard chemical modification of the cationic array in oxides in order to optimize the concentration of anionic carriers, we show that the partial incorporation of F^- anions in fluorinated-hexagonal perovskites (FHP) gives raise to efficient low-temperature O^{2-} mobility. In the Ba/Sr−Fe−O system, fluorides incorporate preferentially highly stable hexagonal [BaF_xO_{3-y}] layers, thus creating extended defected structures. Contrarily to metastable fluorinated-cubic perovskites, FHP show thermal stability above 1000 °C without significant fluoride removal. Such striking stability is made possible by the reversible reorganization of the anionic array (O^{2-}, F^-, and vacancies). It leads to an original "breathing effect" within the hexagonal slabs which improves the redox properties of FHP and suggests a reversible incorporation of oxygen above 200 °C. This phenomenon is rapid and nondestructive as observed from the easy intercalation of FHP-single crystals, fully conserving their crystallinity.

Introduction

Today, amidst growing concerns about diminishing fuel reserves and increasing gas emissions, research on fuel cell technologies is of paramount importance. In particular, the commercial development of solid oxide fuel cells (SOFCs) remains delayed due to one crucial factor. If the working temperature can be reduced from high (800−1000 °C) to intermediate temperatures (500−700 °C), lower manufacturing costs, improved materials compatibility, and long-term durability can all be realized. Lower temperatures require highly mobile anionic species. Two mechanisms are generally proposed in adapted materials to tackle this issue: (a) The access to a lacunar oxygen-network such as in yttrium stabilized zirconia (YSZ), gadolinium doped ceria (CGO), or deficient fluorite structures.[1] (b) Increased interest in materials with interstitial O^{2-} carriers has led to the investigation of alternative structural types for the prospect of next generation electrolytes, scheelite ($CeNbO_{4+x}$),[2] apatite $La_xSi6O_{1.5x+12}$,[3] meilite $(La,Sr)_2Ga_3O_{7+x}$,[4] $La_{1-x}Ba_{1+}GaO_{4-x/2}$,[5] etc. Whatever the nature of carriers is, their concentration and the resulting transport is almost exclusively tuned by aliovalent substitution on the cationic sublattice. One should also consider the possibility of modifying the anionic sublattice for which the aliovalent substitution of O^{2-} for F^- appears ideal, due to their similar ionic radii. We propose here to explore some potentialities of this chemical concept applied on well-adapted materials. It is noticeable that the fluoride incorporation in transition-metal oxides has been developed for a long time, mainly with the aim of modifying their electronic structures (electronic transport and magnetism)[6−8] while the solid-state ionics aspect is rather unexplored. The dimensionality of the anionic diffusion paths is essential and underlies the predominance of perovskite materials in the development of SOFC cathodes. Indeed, high isotropic mixed electronic/ionic transport is favored by their three-dimensional (3D) structural connectivity. Hence, the attention has focused on $La_{1-x}Sr_xMnO_{3-\delta}$[9,10] for its good electronic conductivity, $La_{1-x}Sr_xCoO_{3-\delta}$[11] with enhanced catalytic/ionic activity, and $La_{1-x}Sr_xCo_{1-y}Fe_yO_{3-\delta}$[12] in which the temperature stability

*To whom correspondence should be addressed. E-mail: olivier.mentre@ensc-lille.fr.

(1) Orera, A.; Slater, P. R. *Chem. Mater.* **2010**, *22*, 675–690.
(2) Packer, R. J.; Skinner, S. J.; Yaremchenko, A. A.; Tsipis, E. V.; Kharton, V. V.; Patrakeev, M. V.; Bakhteeva, Yu. A. *J. Mater. Chem.* **2006**, *16*, 3503–3511.
(3) Nakayama, S.; Sakamoto, M.; Highichi, M.; Kodaira, K. *J. Mater. Sci. Lett.* **2000**, *19*, 91–93.
(4) Kuang, X.; Green, M. A.; Niu, H.; Zajdel, P.; Dikinson, C.; Claridge, J. B.; Jantsky, L.; Rosseinsky, M. J. *Nat. Mater.* **2008**, *7*, 498–504.
(5) Kendrick, E.; Kendrick, J.; Knight, K. S.; Islam, M. S.; Slater, P. R. *Nat. Mater.* **2007**, *6*, 871–875.
(6) Mc Cabe, E. E.; Greaves, C. *Fluorine Chem.* **2007**, *128*, 448–458.
(7) Lobanov, M. V.; Abakumov, A. M.; Sidorova, A. V.; Rozova, M. G.; D'yachenko, O. G.; Antipov, E. V.; Hadermann, J.; van Tendeloo, G. *Solid State Sci.* **2002**, *4*, 19–22.
(8) Al-Mamouri, M.; Edwards, P. P.; Greaves, C.; Slaski, M. *Nature (London)* **1994**, *369*, 382–384.
(9) Kuo, J. H.; Anderson, H. U.; Sparlin, D. M. *J. Solid State Chem.* **1989**, *83*, 52–60.
(10) Singhal, S. C. *Solid State Ionics* **2000**, *135*, 305–313.
(11) Teraoka, Y. *Solid State Ionics* **2000**, *48*, 207–212.
(12) Waller, D.; Lane, J. A.; Kilner, J. A.; Steele, B. C. H. *Mater. Lett.* **1995**, *27*, 225–228.

Published on Web 12/06/2010

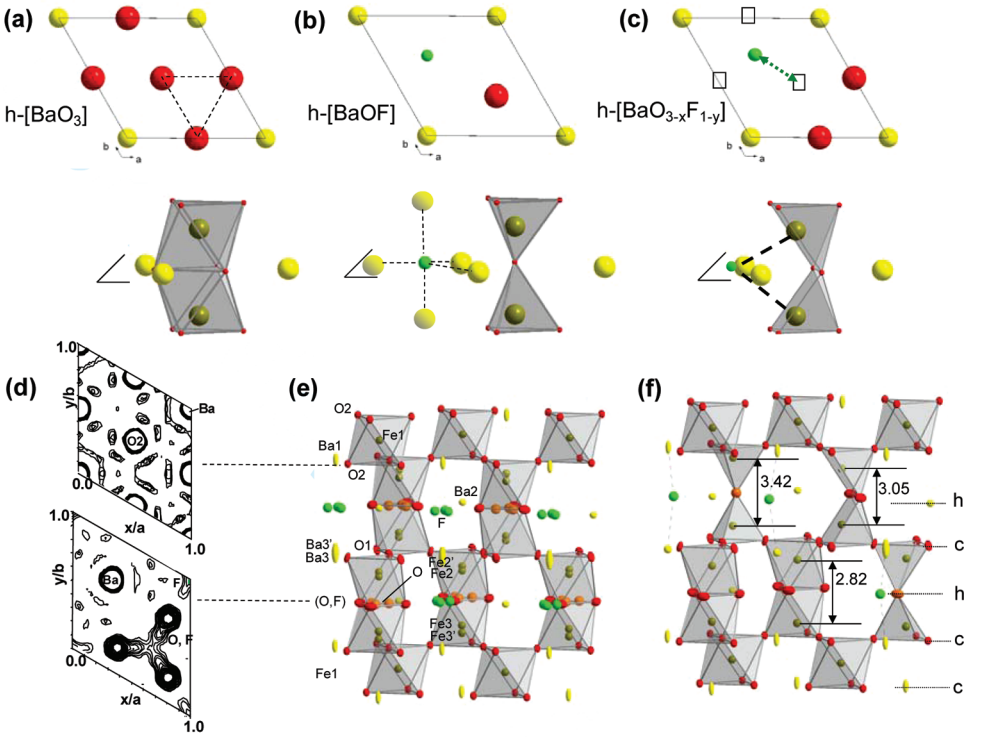

Figure 1. Structural features of FHP. (a) Hexagonal [BaO_3] layers leading to pairs of M_2O_9 face-sharing octahedra at both sides. (b) Ideal [BaOF] layers leading to pairs of corner sharing M_2O_7 and FBa_5 bipyramids. (c) Intermediate degree of fluorination in [$Ba_{3-x}OF_{1-y}$] with the formed M_2O_8 dimer. The dotted arrow shows the relaxed positions for F^-, thus able to move out its Ba5 pyramid into the coordination of the iron cations. (d) 15R-$BaFeF_{0.2}O_{2.44}$ neutron diffraction analysis: Fourier-maps (from observed structure factors) of the cubic (upper) and hexagonal (lower) layers showing an important anionic disorder in the latter. A cutoff was used to mask intensities at the centers of the Ba, O, and F atoms. (e) Single crystal XRD-refined disordered model showing all the located atoms within and out of the hexagonal layers. (f) A possible ordered scheme deduced from the refined model. Fe atoms have been selected from split pairs on the basis of the optimal Fe---Fe distances within the appropriate $Fe_2(O,F)_{9-x}$ group.

is increased. Recently, a number of more "exotic" structural archetypes assorted with lowered dimensionality have emerged, such as the 2D-$Ca_3Co_4O_9$[13] or $RBaCo_4O_{7+\delta}$[14] (R = rare earth), 2D-Ruddlesden−Popper phases,[15,16] or intermediate 2D/3D-$GdBaCo_2O_{5+\delta}$.[17] The goal of our work is to demonstrate, by providing a coherent chemical concept, that partially fluorinated-hexagonal perovskites (FHP) open efficient 2D oxide conduction paths, improving their reactivity with oxygen gas. Particularly, we used iron-based prototypes. The generated strongly defected structures enhance oxygen diffusion through an original mechanism different from the thermally activated anionic-carriers hopping. Our results should stimulate the search for high electrochemical performance in the lacklustre field of hexagonal perovskites.

Experimental Section

Black polycrystalline samples of 15R-$BaFeF_xO_{3-\delta}$ ($0.15 \leq x \leq 0.35$) and 6H-$Ba_{0.8}Sr_{0.2}FeF_xO_{3-\delta}$ ($0.15 \leq x \leq 0.25$) have been obtained through solid-state reaction using stoichiometric mixtures of BaO_2 (Aldrich 95%), SrO_2 (Aldrich 95%), Fe_2O_3 (Aldrich 99%), and BaF_2 (Aldrich 99%) as starting materials. The mixtures were grounded in an agate mortar and placed in closed but not sealed golden tubes. The samples were subsequently heated for 48 h at 900 °C for $BaFeF_xO_{3-\delta}$ and 950 °C for $Ba_{0.8}Sr_{0.2}FeF_xO_{3-\delta}$ and then quenched to room temperature.

Fluoride titration was performed on selected powder samples after dissolution of the compounds, using F specific electrode at the Service Central d'Analyses du CNRS,69360 Solaize, France. Three samples have been selected: "as-prepared" 15R/$x = 0.2$, 15R/$x = 0.15$ and reheated 15R/$x = 0.2$.

Single crystals of the "as-prepared" form were grown using the flux method with BaF_2 as flux agent. A mixture of 90 mol % of BaF_2 and 10 mol % of $BaFeF_xO_{3-\delta}$ powders was placed in an Al_2O_3 crucible, heated up to 1150 °C, and then slowly cooled down to room temperature (5 °C/min). The product was, then, washed with hot water to eliminate the flux and dried. Black single crystals could then be isolated from the final product. For X-ray diffraction (XRD) structural investigations, the same single crystal was collected twice: in its "as prepared" state and after "reheating", in its oxidized form. It was heated at 800 °C for 48 h and quenched to room temperature.

Single crystal XRD data were collected on a Bruker X8 Apex2 CCD4K at room temperature (λ-Mo Kα radiation). The intensities were collected using φ and ω scans and extracted using SAINT program.[18] Intensities were corrected from absorption effects using a semiempirical method based on redundancy with

(13) Nagasawa, K.; Daviero-Minaud, S.; Preux, N.; Rolle, A.; Roussel, P.; Nakatsugawa, H.; Mentré, O. *Chem. Mater.* **2009**, *21*, 4738–4745.
(14) Kadota, S.; Karppinen, M.; Motohashi, T.; Yamauchi, H. *Chem. Mater.* **2008**, *20*, 6378–6381.
(15) Boehm, E.; Bassat, J. M.; Steil, M. C.; Dordor, P.; Mauvya, F.; Grenier, J. C. *Solid State Sci.* **2003**, *5*, 973–981.
(16) Skinner, S. J.; Kilner, J. A. *Solid State Ionics* **2000**, *135*, 709–712.
(17) Tarancon, A.; Skinner, J. S.; Chater, R. J.; Hernàndez-Ramireza, F.; Kilnerb, J. A. *J. Mater. Chem.* **2007**, *17*, 3175–3181.
(18) Area-Detector Integration Software; Siemens Industrial Automation, Inc.: Madison, WI, 1995.
(19) Area-Detector Absorption Correction; Siemens Industrial Automation, Inc.: Madison, WI, 1996.

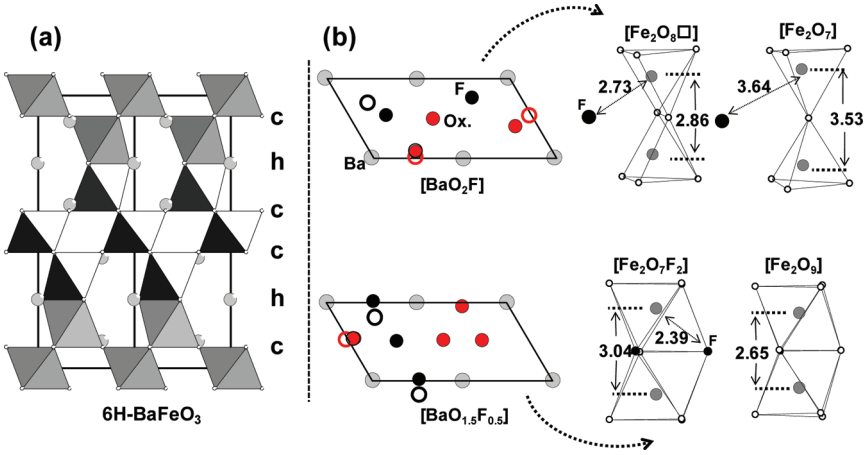

Figure 2. Structural relaxation. (a) Ideal structure of the 6H-$BaFeO_3$. (b) Geometries of the $[BaO_2F]$ (top) and $[BaO_{1.5}F_{0.5}]$ (bottom) layers projected on the (*ab*) plane after full optimization (cell parameters and atomic positions) with corresponding polyhedron dimer geometries beside each layer. Distances are given in (Å). Empty circles represent the ideal position of the corresponding atoms (red for oxygen and black for fluorine) set before optimization.

Table 1. Characteristics and Synthesis of Different Phases in the System Ba−Sr−Fe−O−F

	method	polytype	single-phased x domain	lattice parameters (Å)	red−ox titration
$BaFeF_xO_{3-\delta}$	gold tube	FHP-15R	0.15−0.35	$a \sim 5.75$; $c \sim 36.20$	$x = 0.2$; $\delta = 0.595$; ($Fe^{+3.01}$) $x = 0.25$; $\delta = 0.575$; ($Fe^{+3.10}$) $x = 0.3$; $\delta = 0.64$; ($Fe^{+3.02}$)
	air	FHP-15R + 6H		$a \sim 5.72$; $c \sim 35.81$	
$BaFeO_{3-\delta}$	air	cubic + monoclinic			
	flowing O_2	6H		$a = 5.6753$; $c = 13.9025$	$\delta = 0.1555$; ($Fe^{+3.7}$)
	flowing N_2[36]	monoclinic		$a = 6.919$; $b = 11.726$; $c = 23.623$; $\beta = 98.89°$	
$Ba_{0.8}Sr_{0.2}FeF_xO_{3-\delta}$	gold tube	FHP-6H	0.15−0.25	$a \sim 5.70$; $c \sim 14.30$	$x = 0.2$; $\delta = 0.545$; ($Fe^{+3.11}$)
$Ba_{0.8}Sr_{0.2}FeO_{3-\delta}$	gold tube	6H + cubic			
	air[36]	cubic		$a = 3.998$	
	flowing O_2[36]	cubic		$a = 3.970$	
	flowing N_2[36]	monoclinic		$a = 6.988$; $b = 11.628$; $c = 23.471$; $\beta = 99.10°$	

SADABS program.[19] The crystal structures have been refined using the JANA2000 Software package.[20]

Powder XRD profiles were recorded with a Bruker D8 diffractometer, Cu Kα radiation. High temperature X-ray diffraction (HT-XRD) experiments were carried out on 15R-$BaFeF_{0.2}O_{2.64}$ powder from room temperature up to 1000 °C using an Anton Paar HTK 1200N chamber under flowing air.

Powder neutron diffraction analysis was performed on two samples: $Ba_5Fe_5{}^{+3.04}F_1O_{12.11}$ and $Ba_5Fe_5{}^{+3.08}F_1O_{12.20}$ at the Laboratoire Léon-brillouin (LLB) on the 3T2 diffractometer ($\lambda = 1.2254$ Å). Powder XRD and ND data were analyzed with the Rietveld method using the FULLPROF 2000 program.[21]

Thermogravimetric analysis (TGA) and differential thermal analysis (DTA) were carried out using a combined TG-DTA 92-1600 SETARAM analyzer. Successive heating/cooling cycles were performed using a rate of 5 °C/min. Thermal expansion measurements were performed on 5 mm diameter and ∼10 mm thick pellets; samples were prepared from powders shaped into pellets by uniaxial pressing at 10 MPa and sintering at 900 °C for 24 h in air. The thermal expansion coefficient (TEC) was measured using a Linseis, L75 dilatometer. Three heating/cooling cycles were measured in the temperature range of 50−900 °C.

The oxidation state of iron was determined by a red−ox titration method. The samples were dissolved in a H_3PO_4/H_2SO_4 acidic medium with an excess of Mohr salt. The formal Fe^{4+} reacts with Fe^{2+} leading to Fe^{3+} formation. The amount of remaining Fe^{2+} ions is determined by back-titration with a 0.1 M $KMnO_4$ solution.

O_2-temperature-programmed oxidation experiments (O_2-TPO) were carried out in a Micromeritics Autochem II 2920 equipped with a Thermal Conductivity Detector (TCD), using 5 vol % O_2 in He and a gradual heating rate of 10 °C/min. The outlet gas mixture was simultaneously analyzed using a GEV 010 Omnistar mass spectrometer. Successive cycling between room temperature and 800 °C was performed.

The full geometry optimizations were carried out using the DFT based Vienna ab initio simulation package (VASP) code.[22] The calculations were performed within the generalized gradient approximation (GGA) for the electron exchange and correlation corrections using the Perdew−Wang[23] functional and the frozen core projected wave vector method.[24] A plane wave energy cutoff of 550 eV and 14 *k* points in the irreducible Brillouin zone were used. Structural optimizations converged with residual Hellman−Feynman forces on the atoms smaller than 0.03 eV/Å. The calculations were performed using an antiferromagnetic (AFM) spin configuration for iron atoms.

Incorporation of Fluoride in Hexagonal Perovskites. The broad category of so-called ABO_3 hexagonal perovskites

(20) PetriceK, V.; Dusek, M.; Palatinus, L. JANA2000, The Crystallographic Computing System; Institute of Physics: Praha, Czech Republic, 2000.
(21) Carvajal, R. *J. Phys. B* **1993**, *55*, 192 (program Fullprof available from http://www-llb.cea.fr/fullweb/fp2k/fp2k.htm).
(22) Kresse, G.; Furthmüller, J. Ab-initio Simulation Package (VASP); Institut für Materialphysik: Vienna, 2004; http://cms.mpi.univie.ac.at/vasp.
(23) Perdew, J. P.; Wang, Y. *Phys. Rev. B* **1992**, *45*, 13244.
(24) Kresse, G.; Joubert, D. *Phys. Rev. B* **1999**, *59*, 1758.

(hereafter, A = (Ba,Sr) and B = Fe) have not been included in the quest for promising oxygen-conducting materials. Structurally, the hexagonal perovskites are based on various stacking sequences of closed-packed [AO_3] layers. These sequences include hexagonal (h) close-packing, which leads to face-sharing octahedra of the B cations (for instance, the h-only sequence lead to a 1D-network formed of face-sharing columns ; $BaMnO_3$ archetype, see Figure 1a), and concomitant cubic (c) closed-packing of [AO_3] layers (the c-only sequence leads to the well-known 3D-networks of cubic perovskites with corner-sharing B octahedral; $LaMnO_3$ archetype). In a mixed (h) and (c) stacking sequence, although several examples of preferential creation of oxygen vacancies in the h-layers (see $BaMnO_{3-\delta}$[25] and $BaTiO_{3-\delta}$[26]) are known, no resultant ionic conduction has been reported so far. In such mixed (h) and (c) hexagonal perovskites, the incorporation of halides X^- ($X = F^-, Cl^-$) display their preferential aggregation into hexagonal layers, then leading to O/X ordered hexagonal h′-[$BaOX_{1-\delta}$] layers.[27] It creates B_2O_7 pairs of corner-sharing tetrahedra at both sides of the h′ layer instead of the face-sharing B_2O_9 dimers present in the analogue oxides. In the hexagonal h′-[$BaOX_{1-\delta}$] layers, X is ideally located at the centers of XBa_5 trigonal bipyramids; see Figure 1b. It was shown in two recent $BaCoF_xO_{3-y}$ compounds that the Ba_5 coordination enables a correct compensation of the −1 bond valence of halides by adapted ionic F---Ba bonds,[28,29] while similar OBa_5 pyramids appears rather unlikely.

According to these structural features, the comparison between ideal blocks of hexagonal perovskites of oxides and oxo-fluorides highlights changes of primary importance, as shown in Figure 1a,b. For instance, in the case of the 15R-polytype comprising a part of our study (which ideally corresponds to a unit cell based on 15 layers with the sequence $(cchch)_3$ between [BaO_3] layers), the oxide corresponds to the formula $BaB^{+4}O_3$ against $BaB^{+2.8}F_{0.4}O_{2.2}$ after total fluorination of the h layers. Not only does a strong metal reduction occur but also a drastic dilatation of the hexagonal interleave results from the different B---B interplay. Typically, a distance of 2.5−2.7 Å and 3.3−3.5 Å characterizes the intermetallic separation in these two forms, according to the comparison between various Ba/(Fe,Co) based oxides and oxo-fluorides.[28−31]

A novel permutation would consist of intermediate degrees of fluorination, leading to partially reduced compounds with disordered h-[$BaOF_{1-x}O_{3-y}$] layers. In the hexagonal layers, the existence of oxygen vacancies should favor the shifting of some of the F^- anion into positions intermediate between the ideal centers of the Ba_5 pyramid (see above) and the sphere of coordination of the two apical metals. The compatible area for F^- is shown by a dotted line in Figure 1c. According to the bond valence sum of F^- versus a O^{2-} anions, an apical displacement of the connected metal centers is expected while F^- would participate to the metallic coordination. Then, after partial incorporation of F^- in h layers, variously sized $Fe_2(O,F)_{9-x}$ dimers could cohabit around h layers, once the structural flexibility is adapted to support units of strongly different heights in the same interleaves. Although the existence of such defected structures appears highly unlikely at first glance, their possible properties should be strongly influenced by the high concentration of those local faults, i.e., by the possibility of F^-/O^{2-} and vacancies to reorganize in the layers as the redox is changing.

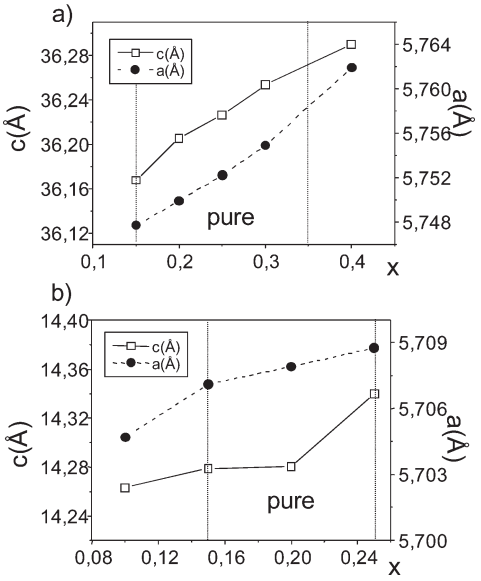

Figure 3. Lattice versus F content. evolution of the hexagonal lattice parameters versus x in (a) the 15R-$BaFeF_xO_{3-\delta}$; a single-phase 15R-polytype ($(cchch)_3$ sequence) is obtained for $0.15 \leq x \leq 0.35$ and (b) the $Ba_{0.8}Sr_{0.2}FeF_xO_{3-\delta}$ 6H-polytypes (chcchc sequence); a single phase is obtained for $0.15 \leq x \leq 0.25$. The increasing of lattice parameters mainly pictures the increasing of tetrahedral coordinated iron sites.

Ab Initio Calculations. These structural predictions have been corroborated by means of density functional theory based geometry optimizations. For reasons of simplification, we performed our calculation on partially fluorinated 6H-hexagonal perovskites which also contains h and c layers according to the (chcchc) stacking sequence. Here, we mainly focus on what is going on during the full-structural relaxation starting from O and F ideal anionic positions, and varying the location of vacancies (see Figures 2 and S1, Supporting Information). It corresponds to a partially fluorinated and oxygen deficient supercell of the 6H-FHP prototype. The calculations have been performed in a $(2 \times a,b,c)$ supercell with the formula $BaFeF_{1/3}O_{2.583}$. Our initial model contains two distinct [BaO_2F] and [$BaO_{1.5}F_{0.5}$] hexagonal layers, F being located at the centers of the Ba_5 bipyramids and replacing face-sharing oxygen atoms, respectively, in the initial model. As expected, after relaxation, the structure covers different Fe−Fe dimers and shows significant shifting of the F^- anions out of their ideal positions. In the same anion-deficient slabs involving [BaO_2F] layers, we note Fe_2O_7 corner-sharing tetrahedra (Fe−Fe = 3.53 Å) and $Fe_2\square_1O_8$ edge-sharing dimers (Fe−Fe = 2.86 Å). In the later, a significant displacement of F^- toward the octahedral vacancy is observed. Around the [$BaO_{1.5}F_{0.5}$] layers, $Fe_2O_7F_2$ (Fe−Fe = 3.04 Å) and Fe_2O_9 (Fe−Fe = 2.65 Å) octahedral pairs are stabilized. This important reorganization within the h blocks is accompanied by slighter but significant displacements of Ba and O atoms inside the surrounding c layers, accommodating severe local constraints and relaxations.

Our choice for the selected chemical systems, namely (Ba,Sr)/Fe/O, follows from recent discoveries: the low-temperature

(25) Adkin, J. J.; Hayward, M. A. *Chem. Mater.* **2007**, *19*, 755–762.
(26) Sinclair, D. C.; Skakle, J. M. S.; Morrison, F. D.; Smith, R. I.; Beales, T. P. *J. Mater. Chem.* **1999**, *9*, 1327–1331.
(27) Darriet, J.; Subramanian, M. A. *J. Mater. Chem.* **1995**, *5*, 543–552.
(28) Ehora, G.; Renard, C.; Daviero-Minaud, S.; Mentré, O. *Chem. Mater.* **2007**, *19*, 2924–2926.
(29) Mentre, O.; Kabbour, H.; Ehora, G.; Tricot, G.; Daviero-Minaud, S.; Whangbo, M. H. *J. Am. Chem. Soc.* **2010**, *132*, 4865–4875.
(30) Delattre, J. L.; Stacy, A. M.; Siegrist, T. *J. Solid State Chem.* **2004**, *177*, 928–935.
(31) Gomez, M. I.; Lucotti, G.; Moràn, J. A.; Aymonino, P. J.; Pagola, S.; Stephens, P.; Carbonio, R. E. *J. Solid State Chem.* **2001**, *160*, 17–24.

Table 2a. Atomic Coordinates and Isotropic Thermal Displacement Parameters for As-Prepared $BaFeF_{0.174}(O,F)_{2.65}$ from Single Crystal XRD Data

atom	wyck./occ.	*x*	*y*	*z*	*U* eq./iso (Å^2)
Ba1	6c/1	0	0	0.13263(2)	0.02071(14)
Ba2	6c/1	1/3	2/3	0.06978(1)	0.01407(11)
Ba3	3a/0.356(2)	0	0	0	0.042(3)
Ba3′	6c/0.322(8)	0	0	−0.01048(11)	0.0059(7)
Fe1	3b/1	1/3	2/3	1/6	0.0089(3)
Fe2	6c/0.668(6)	2/3	−2/3	0.02770(8)	0.0087(3)
Fe2′	6c/0.332(6)	2/3	−2/3	0.02116(15)	0.0087(3)
Fe3	6c/0.747(2)	−1/3	1/3	0.10639(6)	0.0072(2)
Fe3	6c/0.253(2)	−1/3	1/3	0.11674(16)	0.0072(2)
O1	9e/1	1/2	−1.00000	0	0.0185(14)
O2	18 h/1	−0.5003(3)	−0.0005(7)	0.13342(9)	0.0144(9)
		Hexagonal Layer: Anions			
$(O,F)_{Oh}$	18 h/0.627(19)	−0.1925(9)	0.1925(9)	0.06804(18)	0.032(3)
O_{Td}	18 h/0.086(17)	−0.279(6)	0.279(6)	0.0663(13)	0.028(13
F_{Ba5}	18 h/0.145(15)	0.041(6)	−0.041(6)	0.0647(11)	0.08(2)

Table 2b. Selected Bond Distances (Å) for the Single Crystal of the As-Prepared $BaFeF_{0.174}(O,F)_{2.65}$[a]

atoms	*d* (Å)
Fe1−O2 (×6)	2.033(3)
$Fe2_{Oh}$−O1 (×3)	1.926(1)
$Fe2_{Oh}$−$(O,F)_{Oh}$ (×2 or ×3)	2.008(8)
$Fe2_{Td}$−O1 (×3)	1.926(1)
$Fe2_{Td}$−O_{Td} (×1)	> 1.481(9)*
$Fe3_{Oh}$−O2 (×3)	1.916(10)
$Fe3_{Oh}$−$(O,F)_{Oh}$ (×3)	1.958(7)
$Fe3_{Td}$−O2 (×3)	1.879(3)
$Fe3_{Td}$−O_{Td}	> 1.531(5)*
Fe2−Fe3	2.817(9)
F_{Ba5}−Ba2 (×3)	2.902(2)−3.528(3)
F_{Ba5}−Ba1	2.466(5)
F_{Ba5}−Ba3′	2.722(4)

[a] The distances noted with an ∗ are too short due to the bad localization of Fe2 and Fe3 in their tetrahedral coordination, masked by their thermal vibration along *c*.

oxygen mobility in three-dimensional $SrFeO_{3-x}$ perovskites[32] and their topotactic reduction leading to the two-dimensional anion-deficient $SrFeO_2$ end-member.[33] Also, the cubic stabilized $BaFeO_{3-\delta}$ phases demonstrate significant oxygen permeation through dense membranes.[34] Finally, the $BaFeO_{3-\delta}$ system displays an impressive number of polytypes that are stabilized along the δ anionic nonstoichiometry.[35,36] About the fluorination effect in this chemical system, recent studies show that the topotactic fluorination of cubic-related Ba/Sr−Fe perovskites at moderate temperature (400 °C) yields metastable cubic $(Ba,Sr)FeO_2F$ compounds.[36] What about the role of hexagonal layers in Ba−Fe FHP?

We achieved the successful preparation of hexagonal-FHP using high temperature synthesis from BaF_2 precursor in sealed gold tubes; see Table 1. In this table, we also report related compounds of various compositions, which highlight the drastic role of the elaboration process in this versatile chemical system. Using our synthesis method, the $BaFeF_xO_{3-\delta}$ composition leads to the single-phased 15R-polytype ($(cchch)_3$ sequence) for $0.15 \leq x \leq 0.35$. In absence of fluor, this form was only evidenced via a significant substitution of iron for a tetravalent cation (Ir^{4+}, Mn^{4+}).[37,38] We also used a 20% Ba for Sr replacement to obtain the pure $Ba_{0.8}Sr_{0.2}FeF_xO_{3-\delta}$ 6H-polytype (chcchc sequence) for $0.15 \leq x \leq 0.25$. Without additional thermal treatment, the corresponding tube-prepared samples are denoted as-prepared compounds and have a mean iron oxidation state of about +3, according to our permanganate redox titrations; see Table 1. Their lattice parameters increase with *x*, as expected from the growing contribution of the big-sized Fe_2O_7 tetrahedra pairs in the h slabs in addition to the reduction effect of Fe^{4+} into Fe^{3+}, Figures 3 and S2 (Supporting Information). It is clear that the lattice evolution versus *x* is more continuous for the 15R-FHP than for the 6H-FHP in probable relation with the highest concentration of modifiable h layers in the total stacking sequence for the former, i.e., 2/5 for the 15R-FHP ($(cchch)_3$ sequence) against 2/6 for the 6H-FHP ((chcchc) sequence). Also, we checked that the nominal values of incorporated fluorides are well conserved in the final as-prepared compounds: For as-prepared 15R-phases with $x = 0.15$ and 0.2, the elemental analysis (F/Ba/Fe) and redox titration leads to the formulas $BaFe^{+3.01}F_{0.14}O_{2.57}$ and $BaFe^{+3.10}F_{0.19}O_{2.46}$, respectively. With reasonable certainty, the deviation between the incorporated and titrated F^- amount is sufficiently low to consider a total incorporation in the final product.

Extended Defect Structure. Structural Rietveld refinements from neutron diffraction (ND) data collected at room temperature on several 15R-samples give information on the typical disordered features of the FHP (Figure S3, Supporting Information). It is detailed below for the $15R/x = 0.2$ compound with the final formula $BaFe^{+3.08}F_{0.2}O_{2.44}$ ($a = 5.74324(1)$ Å, $c = 36.093(1)$ Å, space-group $R\bar{3}m$, $R_{Bragg} = 8.27\%$). One major difficulty in the refinements arises from the disordered character of the structure assorted with the antiferromagnetic ordering between Fe atoms even at room temperature. The magnetic structure, not concerned here, will be presented elsewhere. (a) In the 3D-edifice of the 15R-FHP, the coordination of the iron located (see Figure 1f) between two cubic c layers forms regular octahedra with six Fe1−O2 distances of ∼2.045 Å, compatible

(32) Paulus, W.; Schober, H.; Eibl, S.; Johnson, M.; Berthier, T.; Hernandez, O.; Ceretti, M.; Plazanet, M.; Conder, K.; Lamberti, C. *J. Am. Chem. Soc.* **2008**, *130*, 16080–16085.
(33) Tsujimoto, Y.; Tassel, C.; Hayashi, N.; Watanabe, T.; Kageyama, H.; Yoshimura, K.; Takano, M.; Ceretti, M.; Ritter, C.; Paulus, W. *Nature* **2007**, *450*, 1062–1065.
(34) Kida, T.; Takauchi, D.; Watanabe, K.; Yuasa, M.; Shimanoe, K.; Teraoka, Y.; Yamazoea, N. *J. Electrochem. Soc.* **2009**, *156*, E187–E191.
(35) Grenier, J. C.; Wattiaux, A.; Pouchard, M.; Hagenmuller, P.; Parras, M.; Vallet, M.; Calbet, J.; Alario-Franco, M. A. *J. Solid State Chem.* **1989**, *80*, 6–11.
(36) Clements, O.; Haberkorn, R.; Slater, P. R.; Beck, H. P. *J. Solid State Sci.* **2010**, *12*, 1455–1463.
(37) Jordan, N. A.; Battle, P. D.; Sloan, J.; Manuel, P.; Kilcoyne, S. *J. Mater. Chem.* **2003**, *13*, 2617–2625.
(38) Cussen, E. J.; Sloan, J.; Vente, Battle, P. D.; Gibb, T. C. *Inorg. Chem.* **1998**, *37*, 6071–6077.

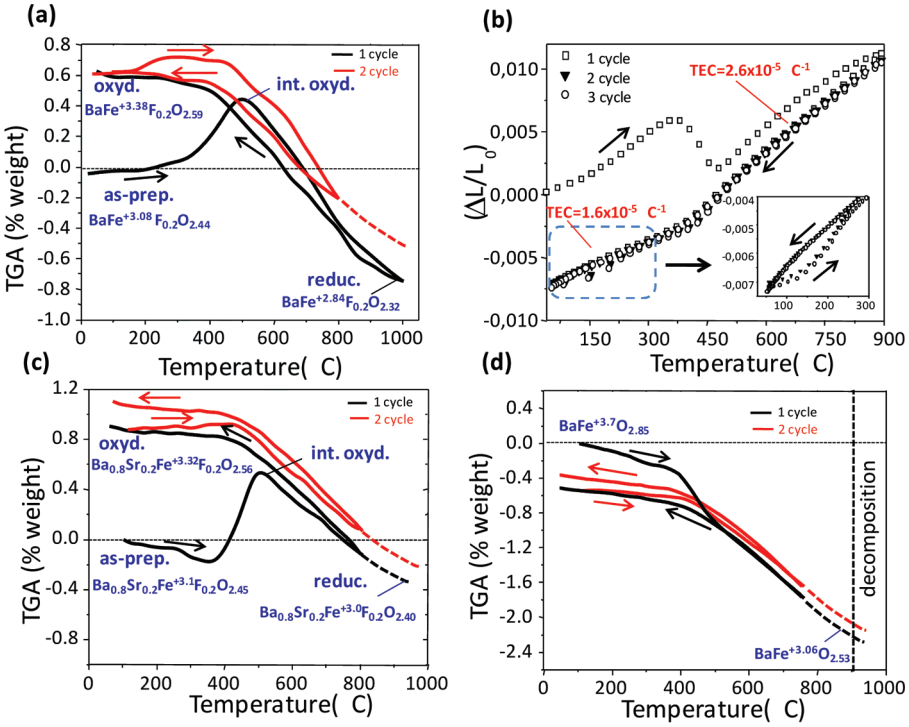

Figure 4. Thermal behavior of FHP and related oxides. TGA under flowing air, in two subsequent heating/cooling cycles, and deduced formulas of the as-prepared (from redox titration), reduced, and oxidize forms starting from (a) 15R-$BaFeF_{0.2}O_{\sim 2.44}$ (note the oxidation reactions starting at 200 °C even upon the second heating, (c) 6H-$Ba_{0.8}Sr_{0.2}FeF_{0.2}O_{\sim 2.45}$ (weakest second reoxidation than in the 15R-form), (d) 6H-BaFeO ~ 2.85 (no low temperature phenomena). (b) Thermal dilatometry under three subsequent heating/cooling cycles for the 15R-$BaFeF_{0.2}O_{\sim 2.44}$ with the thermal expansion coefficient (TEC) values of the oxidized form (below 450 °C) and reduced form (above 450 °C). Upon the first heating, the dilatation combines the first oxidation process (lattice contraction) and the densification of the sample. The next cycles are fully reproducible even for the low-temperature contraction (see the inset).

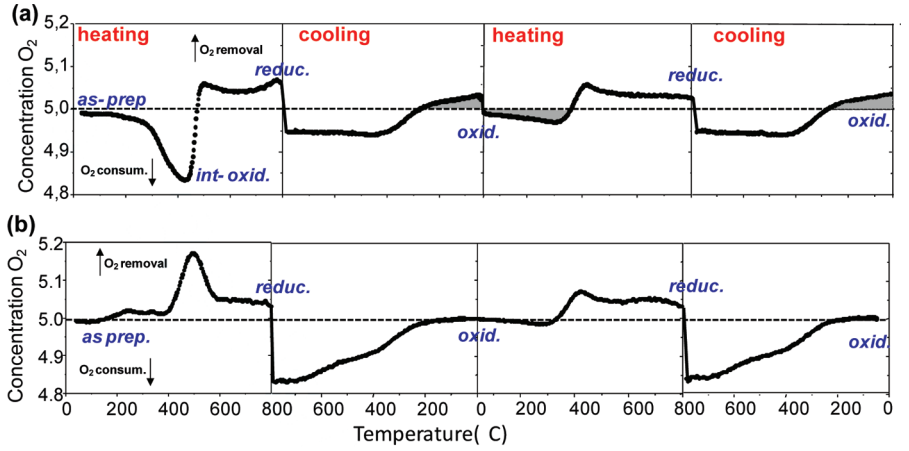

Figure 5. Evidence of low temperature solid−gas reactions: Temperature programmed oxidation (TPO) profiles against temperature under flowing 5% O_2−95% He, after normalization for identical number of iron cations. (a) 15R-$BaFeF_{0.2}O_{3-\delta}$ with indication of the as-prepared, intermediate-oxidized, reduced, and oxidized states. (b) 6H-$BaFeO_{3-\delta}$ following two subsequent heating/cooling cycles. The deviation from the 5% line shows O_2 consumption (down) or removal (up). In the FHP, the zones in gray highlight the striking low-temperature oxidation (on heating) and reduction (on cooling) processes while more regular high temperature exchanges are evidenced for the FHP than for the oxide.

with Fe^{3+}---O bonds (bond valence sum = 2.77). Contrarily to what is observed in the cubic fluorinated $BaFeO_2F$ compound,[39] the absence of high thermal parameters for the corner sharing anions implies no significant incorporation of fluor in the c layers but strongly suggests their preferentially incorporation in the h layers. (b) As expected from our calculations, an important anionic disorder inside the h layers was evidenced, as shown on the corresponding Fourier-difference maps (broad nucleon density around the ideal anionic positions), Figure 1d. This distribution was modeled by two sets of anionic crystallographic positions statically disordered in the crystals. The first one (O_{Td}) relates to shared corners of the Fe_2O_7 dimers (Figure 1b). The second one ($(O,F)_{Oh}$) is associated with more or less anionic-deficient face sharing $Fe_2O_6(O,F)_{3-x}$ octahedral dimers (Figure 1a,c). In the concerned 15R-$BaFe^{+3.08}F_{0.2}O_{2.44}$ compound, about 7% $Fe_2(O,F)_9$, 52% $Fe_2(O,F)_8$, and 21% Fe_2O_7 have been deduced by means of ND and redox titration.

(39) Heap, R.; Slater, P. R.; Berry, F. J.; Helgason, O.; Wright, A. J. *Solid State Commun.* **2007**, *141*, 467–470.

(c) A significant F^- presence is detected at the centers of the Ba_5 triangular pyramids. As already argued, the existence of these sites is correlated with the presence of Fe_2O_7 dimers, as observed around ideal [BaOF] layers, Figure 1b. (d) In such disordered hexagonal-slabs, the thermal displacement for all cations is exaggerated along the *c* axis, some of them being even split into two next-positions to cover the broad nucleon density. It pictures an important diversity of local configurations and demonstrates the high flexibility of hexagonal lattices after fluorination. A more accurate characterization of this disorder was reached through XRD analysis of "as-prepared" single crystal (Figure S3, Supporting Information). The final refined composition is $BaFeF_{0.17}(O,F)_{2.64}$, space group $R\bar{3}m$, $a = 5.7196(2)$ Å, $c = 35.8050(13)$ Å, $R_{F(all)} = 2.87\%$, $wR_{F(all)} = 2.73\%$. In the above formula, F represents the anions at the center of the Ba_5 pyramids which are unambiguously assigned to F, (O, F) tetrahedral and octahedral oxygen corners which could include a part of F^- displaced in the coordination sphere of the iron sites inside the h layers. The atomic positions and pertinent distances are listed in Tables 2a and 2b. Figure 1e shows the disordered refined model, which would ideally correspond to the superposition of variable local configurations as shown in Figure 1f. The presence of two split sites for the iron in the h blocks leads to a distribution of Fe---Fe distances, between the short 2.817(4) Å and the long 3.422(8) Å separations. They can, in a first approximation, picture octahedral and tetrahedral pairs, respectively. For intermediate configurations (pyramidal pairs), the distance should be somewhere between 2.8 and 3.4 Å. The high thermal anisotropy and/or split of most of the barium atoms also reflects various local positions which depends, for instance, on the presence or the absence of F^- in their coordination sphere. The cohabitation of so-different units creates an extended defected structure with a distribution of constrained and relaxed sites. The resulting structural fluctuation is expected to open important channels for oxygen diffusion, as discussed below.

Thermal Stability of FHP. Taking into account the general unstability of oxofluoride materials, it is striking that no significant fluoride loss has been evidenced for FHP on TGA coupled with mass spectrometry until 1000 °C in air. In addition, in situ high temperature XRD experiments on the as-prepared FHP systematically show the conservation of the original single-phase materials, with lattice modifications arising from the oxygen stoichiometry only (for $x = 0.2$ and 0.25, Figure S4, Supporting Information). Finally, the fluor titration of the 15R-$BaFeF_{\sim 0.2}O_{2.44}$, after a 2 day thermal treatment at 900 °C in air shows an evolution of the titrated fluor from $x = 0.19$ (as-prepared) to 0.18 (after treatment). The strong thermal stability of FHP is reminiscent of cobalt oxochloride and oxofluorides hexagonal polytypes, in which similar high temperature stability was observed above 1000 °C.[29,40,41] This striking stability of the halides in h-$[BaOF_{1-x}O_{3-y}]$ layers is to oppose to the metastable character of the cubic compounds obtained after topotactic fluorination of the $AFeO_{3-\delta}$ oxides. Indeed, such cubic-$AFeO_2F$, A = Ba/Sr, decompose around 750 °C yielding (Ba/Sr)-F_2 salts.[36] To check this point about the high-stability of F^- in hexagonal slabs, we prepared using our experimental protocol the single-phased $Ba_{0.2}Sr_{0.8}FeF_xO_{3-x-\delta}$ with $x = 0$ (cubic) and $x = 0.1$ (tetragonal, pseudocubic) which only contain $[Ba(O,F)_{3-x}]$ cubic layers. For $x = 0.5$, after the first heating/cooling ramp, the lattice parameters finally coincide with those of the cubic $x = 0$ oxide, which comforts the removal of main of the initial fluoride content after their insertion in the cubic layers (Figure S5, Supporting Information). Here, the preferred location and higher thermal stability of F^- in h layers rather than cubic ones most probably arises from the strong constraints involved in corner sharing B--F--B units. As the bond valence sum is commonly defined by $S_{ij} = \Sigma_j \exp[(R_{ij} - dij)/0.37]$,[42] it is clear that the replacement of O^{2-} ($S = -2$, $R_{O-FeIII} = 1.759$) for F^- ($S = -1$, $R_{F-FeIII} = 1.67$) leads to a dilatation of the mean Fe---F distances. This should be responsible for severe local constraints in a (pseudo)-cubic network, while deficient hexagonal $[BaOF_{1-x}O_{3-y}]$ layers offer possibilities for "in-plane" relaxation by shifting the F^- anions (see Figure 1c). Also, following the method described in ref 43, we prepared the 6H-$BaFeO_{\sim 2.85}$. In situ-high temperature XRD shows its transformation into the cubic-$BaFeO_{3-\delta}$ polytype around 900 °C while no degradation was evidenced on heating/cooling cycles for the 6H-FHP up to 1000 °C. The stabilization of the hexagonal polytypes after incorporation of fluor is demonstrated.

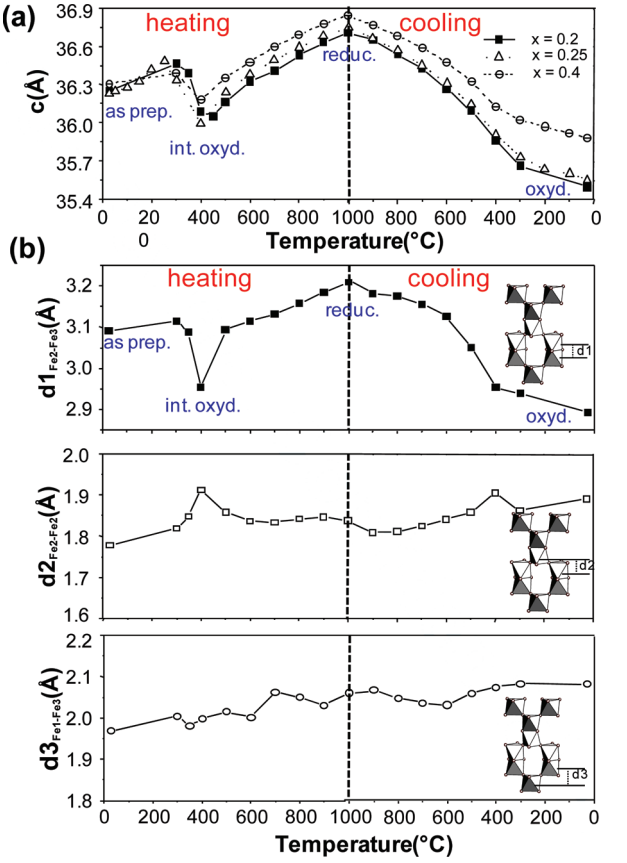

Figure 6. "Breathing" of the FHP-hexagonal slabs: (a) c-lattice parameter versus temperature for 15R-$BaFeF_xO_{3-\delta}$ upon heating/cooling. Thermal evolution of the intermetallic separations projected on the *c*-axis: (b) intrahexagonal slab Fe2−Fe3, (c) cubic-to-hexagonal Fe2−Fe2, and (d) cubic-to-hexagonal Fe1−Fe3.

Low Temperature Oxygen Gas−Solid Transfer. The as-prepared 15R-FHP and 6H-FHP have been analyzed on the basis of TGA, in situ high temperature XRD, dilatometry, and temperature programmed oxidation (TPO, under 5% O_2−95% He flowing atmosphere), offering up precise insights about the solid−gas exchanges; see Figures 4 and 5. For both polytypes,

(40) Kauffmann, M.; Mentré, O.; Legris, A.; Hébert, S.; Pautrat, A.; Roussel, P. *Chem. Mater.* **2008**, *20*, 1741–1749.
(41) Mentre, O.; Kauffmann, M.; Ehora, G.; Daviero-Minaud, S.; Abraham, F.; Roussel, P. *Solid State Sci.* **2008**, *10*, 471–475.
(42) Brese, N. E.; O'Keeffe, M. *Acta. Crystallogr.* **1991**, *B47*, 192–197.
(43) Mori, K.; Kamiyama, T.; Kobayashi, H.; Oikawa, K.; Otomo, T.; Ikeda, S. *Phys. Soc. Jpn.* **2003**, *72*, 2024–2028.

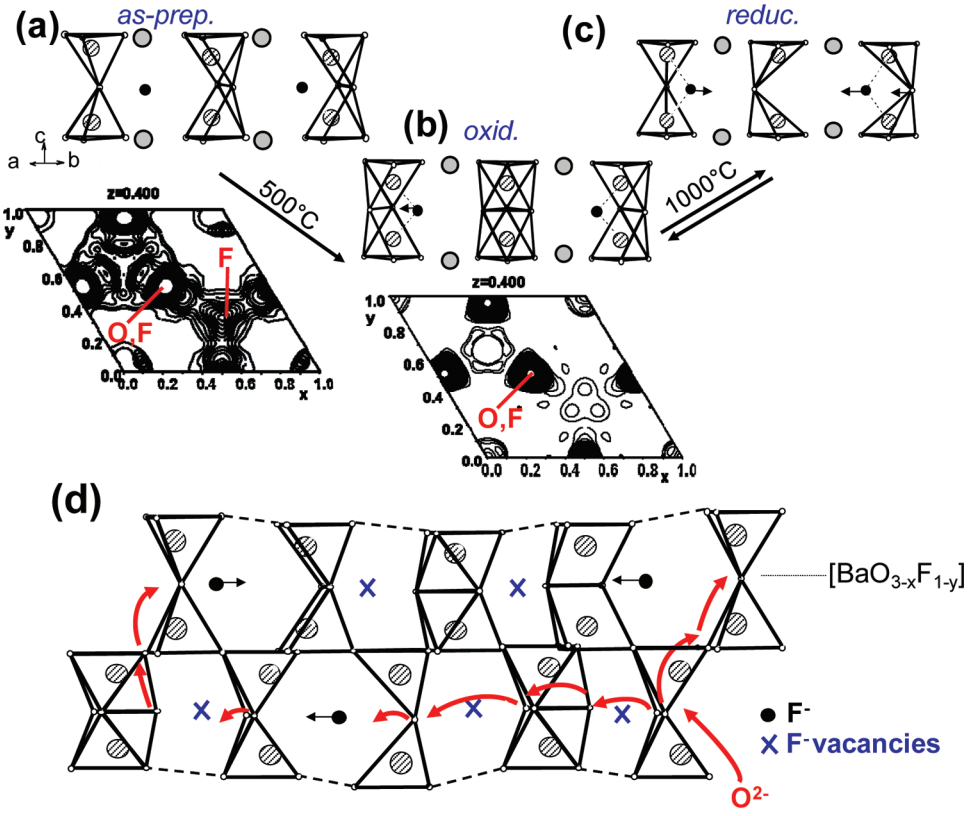

Figure 7. Structural rearrangement of fluorinated-hexagonal layers as the redox changes. (a) Distribution of several types of $Fe_2(O,F)_{9-x}$ in the as-prepared state, from powder-ND and singe crystal XRD experiments. The Fourier-difference map of hexagonal layers in absence of the anions (single crystal data) shows the disorder. (b) Oxidized state (from reheated single crystal data) with increasing number of octahedral configuration while F in the Ba_5 pyramids are not significantly evidenced in the corresponding Fourier-difference map. (c) Predominance of the distorted tetrahedral configurations in the reduced state, from high-temperature in situ XRD. (d) A possible mechanism of oxide migration and F^- displacements activated by structural fluctuations.

on the first heating ramp, a broad oxidation reaction takes place from 200 to 500 °C within the limits of the experimental sensibility and of the thermal stability (from as-prepared to intermediate-oxidized states) immediately followed by a monotone important reduction (from intermediate-oxidized to reduced states). These two phenomena are accompanied by subsequent drastic lattice contraction and expansion, respectively, Figures 4b and 6. For the 15R/x = 0.2 sample, according to the TGA curve, the corresponding formula and iron valence would correspond to as-prepared $BaFe^{+3.08}F_{0.2}O_{2.44}$ at room temperature → intermediate-oxidized $BaFe^{+3.3}F_{0.2}O_{2.55}$ at 500 °C → reduced $BaFe^{+2.84}F_{0.2}O_{2.32}$ at 1000 °C. The TPO profile of the 15R/x = 0.2 shows a broad O_2 consumption peak and a O_2 removal plateau associated with these two phenomena. Here, one should recall that, since the signal shows the concentration of O_2 at the detector after flowing through the sample, a plateau involves a constant removal or incorporation of oxygen. Then, it is in good adequation with the linear increase/decrease of the TGA in the same temperature range. The first oxidation phenomenon brings important insight about the feasibility of low temperature gas−solid exchanges since it starts around 200 °C. As expected, this phenomenon is accompanied by a drastic anomaly of the thermal expansion measured by dilatometry, Figure 4b.

After this first heating ramp, upon further cooling, a reoxidation process is observed up to 200 °C by TGA, while the materials return to their oxidized states. It is noteworthy that, for the 15R/x = 0.2 compound, the TPO profile shows that the corresponding O_2 consumption is followed by a significant release of O_2 apparent below 200 °C and shown in gray in Figure 5. Of course, a drifting temperature effect could reasonably generate such an artifact, and one should carefully consider the low-temperature data. However, the absence of such phenomenon for the 6H-$BaFeO_{3-\delta}$ (Figure 5b) still suggests the particular role of the fluorinated h layers.

Additional heating/cooling treatments are reversibly cycled between the oxidized and reduced states, but a weaker sensitive weight gain (~0.15%) reappears around 200 °C on the second heating, most pronounced for the 15R-FHP than for the 6H-FHP. For the 15R- compound, significant consumption/removal of O_2 are reproducibly observed below 200 °C on heating/cooling ramps on TPO profiles, once more possibly arising from thermal drifting effects. In this particular compound, the high concentration of hexagonal layer (=2/5 of the total number of layers) combined with the fluoride content could be a key factor. This potential low-temperature (T < 200 °C) oxidation/reduction is accompanied by lattice contraction/expansion, which was observed by dilatometry on the second and third thermal cycles on which a significant heating/cooling divergence is evidenced; see the inset of Figure 4b. On the contrary, the 6H/x = 0.2 FHP, TPO did not reveal significant temperature gas-exchange in the second cycle below 200 °C (Figure S6, Supporting Information), maybe due to the lowest concentration of hexagonal layers (=2/6).

The comparison with the behavior of the 6H-oxide enables one to distinguish the particular role of fluorination. For this oxide, both TGA (Figure 4d) and TPO (Figure 5b) emphasize an important reduction phenomenon starting at 400 °C on heating (from 6H-$BaFe^{+3.87}O_{\sim 2.85}$ at room temperature to 6H-$BaFe^{+3.06}O_{\sim 2.53}$ at 800 °C), while additional cooling/heating cycles show a reversible standard reduction/reoxidation

Table 3a. Atomic Coordinates and Isotropic Thermal Displacement Parameters for the Oxidized-$BaFeO_{1.8}[(O,F)_{0.86}]_{hex}$

atom	wyck./occ.	*x*	*y*	*z*	*U* eq./iso[a] (Å^2)
Ba1	6c/1	0	0	0.13225(2)	0.0154(3)
Ba2	6c/1	1/3	−1/3	0.06893(2)	0.0156(2)
Ba3	6a/0.5	0	0	0.00734(5)	0.0197(6)
Fe1	3b/1	1/3	2/3	1/6	0.0118(6)
Fe2	6c/1	2/3	1/3	0.02733(5)	0.0175(5)
Fe3	6c/0.901(4)	2/3	1/3	0.10706(5)	0.0110(5)
Fe3b	6c/0.1107(6)	2/3	1/3	0.1311(5)	0.0110(5)
O1	9e/1	0	−1/2	0	0.022(2)
O2	18 h/1	0.1660(5)	−0.1660(5)	0.20003(13)	0.0177(16)
		hexagonal layer: anions			
$(O,F)_{Oh}$	18 h/0.8981(8)	−0.1866(9)	0.1866(9)	0.06752(19)	0.038(3)

[a] Note: Fe3b (occupancy = 11%) is shifted toward the centers of the apical triangular faces of the dimers. It corresponds to Fourier-difference peak of $\pm 10e^-/Å^3$ which has been systematically observed in our several diffraction experiments on reheated crystals (under air, under oxygen, quenched or not). The Fe3b−O distances (= 1.65 Å) are not realistic but show the trend for the shifting of the Fe3 cations due to their important coordination by fluoride in the octahedra.

Table 3b. Selected Bond Distances (Å)a

atoms	*d* (Å)
Fe1−O2 (×6)	2.031(4)
$Fe2_{Oh}$−O1 (×3)	1.908(1)
$Fe2_{Oh}$−$(O,F)_{Oh}$ (×2 or ×3)	2.034(7)
$Fe3_{Oh}$−O2 (×3)	1.885(4)
$Fe3_{Oh}$−$(O,F)_{Oh}$ (×3)	2.014(7)
Fe2−Fe3	2.826(3)

[a] Fe3b (11% occupied position) was excluded (Fe3b---O = 1.65 Å) from the list.

between $BaFe^{+3.06}O_{\sim 2.53}$ and $BaFe^{+3.54}O_{\sim 2.77}$. No significant phenomenon is observed below 400 °C. The role of fluor insertion in FHP on the low temperature heating/cooling divergences is, thus, unambiguously established. Furthermore, the comparison of the profiles of the TPO reoxidation processes between 6H-oxide and 15R-FHP gives new insights. The variation of the O_2 concentration at the detector is erratically varying vis-a-vis temperature for the 6H-$BaFeO_{3-\delta}$, in contrast to the flat plateau (400−800 °C) in the 15R-FHP. It strongly suggests a more controlled and regular driving exchange process, fully compatible with the creation of ionic conductor pathways in hexagonal blocks of the FHP. Under the restrictions due to experimental errors mentioned above, the activation of the gas−solid transfer below 300 °C is a striking result. This threshold coincides with temperature for free oxygen mobility in the relevant $SrFeO_x$ ($2.5 \leq x \leq 3.0$).[32] In this latter system, the mechanism for the topotactic reversible intercalation reaction relies on the specific low-energy lattice mode, which triggers and amplifies oxygen mobility at low temperatures. In contrast, the reversible mechanism occurring in FHP most certainly is due to extended defect structure inside the fluorinated-hexagonal blocks.

Proposed Mechanism. In situ high temperature XRD structural analyses of the 15R-as-prepared $x = 0.2$ sample on heating/cooling from room temperature to 1000 °C enables the quantification of the structural fluctuation between the oxidized and reduced states (Figures S7 and S8, Supporting Information). Special attention was paid to the cationic array for which accurate information was possibly obtained from XRD data. The thermal evolution of the projection of the mean Fe--Fe separation along the *c* axis was analyzed; see Figure 6. It appears immediately that the Fe2---Fe3 (inside the h slabs) is fully responsible for most of the thermal lattice changes, i.e., the drastic contraction and dilatation effects upon the oxidation and reduction, respectively. The Fe---Fe distance changes from 2.88 Å (oxidized, at room temperature) to 3.21 Å (reduced, at 1000 °C). It corresponds to a giant Fe---Fe dilatation coefficient $\Delta d/(d_0 \Delta T)$ of 118.10^{-6} °C^{-1} to compare to the bulk-thermal expansion of 15.10^{-6} °C^{-1} (below 400 °C) and 26.10^{-6} °C^{-1} (above 400 °C), Figure 4b. This "breathing" phenomenon within the hexagonal slabs certainly arises from the capacity of the system to accommodate a variety of environments for the iron cations in a reversible way versus temperature, while the F^- anions are concomitantly displaced from Ba_5 to the iron coordination. This is schematized in Figure 7a as deduced from several structural analyses (single crystal of as-prepared and oxidized-forms, in situ powder XRD data of the reduced form at 1000 °C; Figure S8, Supporting Information). Here, the distribution of $M_2(O,F)_{9-x}$ units with different sizes is expected to generate extended fluctuations in the h slabs, activating easy in-plane oxygen diffusion assisted by reversible modifications of the iron environment, Figure 7b. The degree of freedom of F^- is expected to be restrained to short displacements from F--Ba_5 to F--Fe, regarding its cationic avidity. At the very least, we have clearly established the stability in the structure at high temperature of fluoride after their incorporation in the hexagonal blocks. It has also been possible to precisely probe the oxidized state, after heating to 800 °C in air and rapid cooling, the single crystal already described above in its as-prepared state (as-prepared state: formula = $BaFeF_{0.17}(O,F)_{2.64}$, a = 5.7196(2) Å, c = 35.8050(13) Å, $R_{F(all)}$ = 2.87%, $wR_{F(all)}$ = 2.73%). Strikingly after heating, the crystallinity was fully conserved while the structure has evolved (oxidized state: formula = $BaFe(O,F)_{2.88}$, a = 5.7011(5) Å, c = 35.4219(14) Å, $R_{F(all)}$ = 2.94%, $wR_{F(all)}$ = 2.82%). Furthermore, even with conservative consideration of the refined occupancies of the anionic positions from XRD data, our refinements confirm the oxygen gain and the lattice contraction after heating in air. Especially, it appears from difference Fourier maps of the hexagonal layers that a total migration of O/F anions into octahedral-corner positions, in order to incorporate extra O^{2-} anions, takes place. The atomic positions and pertinent distances in the oxidized form are listed in Tables 3a and 3b. With the full intercalation of dense single crystal being generally slow, one could expect a fast and efficient oxide-transport process in FHP even at low temperature. However, one should mention the appearance of a residual peak ($\sim 10e^-/Å^3$) on final Fourier difference at the center of the external O_3 face of the dimers (coordinates: 1/3, 2/3, ~0.13). The resulting MO_3 polyhedra with three M−O distances of ~1.65 Å appears rather incompatible with any of the present elements. However, it was assigned to partially filled iron position (Fe3b, occupancy = 11%) and pictured a trend for an apical shifting of some Fe3 cations

(ideal coordinates: 1/3, 2/3, ~0.10) in their octahedra, arising during the rearrangement of the (O,F) anions within the h layers. Several crystals of the initial preparation have been reheated under air and collected . They systematically show this strong residual density. Its full understanding is still under progress.

Concluding Remarks

We show that the partial incorporation of F^- in (Ba,Sr)/Fe based hexagonal perovskites yields extended defect structures which show reversible removal/incorporation of oxygen and possible ionic conductivity even at low temperature ($T > 200$ °C). From our structural characterizations, this phenomenon would be driven by a giant "breathing phenomenon" which accompanies the reorganization of the anionic (O,F) subarray versus temperature and the concomitant rearrangement of iron coordination. This original/striking process takes place in the hexagonal slabs, which can be considered as 2D subunits of the structure. It opens wide prospective fields for new efficient ionic conducting oxides. In this aim, the original targeted modification of the anionic subarray appears strongly efficient at low temperature. Especially, the conductivity mechanism within the h slabs implies fine structural rearrangements inside extended defect structures. About the materials selected here, even if 3D-perovskite archetypes continue to dominate the literature in this field, we show new potentialities of the alternative broad family of hexagonal perovskites, not included in this quest so far. Taking into account the structural diversity reachable by chemical modification of the ideal ABX3 formulation, one should realize the potentiality for further investigation out of the (Ba,Sr)/Fe/(O,F) system. Especially, according to a modular structural description, the fluorinated-hexagonal slabs could be considered as efficient 2D-ionic conducting blocks, located between interchangeable modules which could bring their own specificities and intrinsic properties.

Acknowledgment. The authors are grateful to Florence Porcher (LLB, Saclay, France) for her help in ND data collection and to Mousumi Mukerji for her help in the writing process.

Supporting Information Available: Details of ab initio calculations, neutron diffraction (ND), XRD analysis of single crystal and in situ high temperature of powders, and heating/cooling ramps on TPO profiles for several 15R-FHP samples; additional figures as noted in the text (PDF, CIF). This material is available free of charge via the Internet at http://pubs.acs.org.